Aging Study on the Structure of Fe 0 Nanoparticles: Stabilization, Characterization, and Reactivity

ARTICLE *in* THE JOURNAL OF PHYSICAL CHEMISTRY C · FEBRUARY 2010

Impact Factor: 4.77 · DOI: 10.1021/jp909137f

3 AUTHORS, INCLUDING:

Qiliang Wang
Rice University
14 PUBLICATIONS **434** CITATIONS
SEE PROFILE

Heechul Choi
Gwangju Institute of Science and Technology
156 PUBLICATIONS **4,352** CITATIONS
SEE PROFILE

Aging Study on the Structure of Fe^0-Nanoparticles: Stabilization, Characterization, and Reactivity

Qiliang Wang,[†] Sanghyup Lee,[‡] and Heechul Choi*,[†]

Department of Environmental Science and Engineering, Gwangju Institute of Science and Technology (GIST), 261 Cheomdan-gwagiro, Buk-gu 500-712 Gwangju, Korea, and Center for Environmental Technology Research, Korea Institute of Science and Technology, 130-650 Seoul, Korea

Received: September 23, 2009; Revised Manuscript Received: December 14, 2009

Inert/pseudoinert gases, including argon, nitrogen, and carbon dioxide, were utilized to stabilize synthesized Fe^0-nanoparticles after lyophilization to prevent self-ignition. In addition, the aging effect was investigated for these stabilized Fe^0-nanoparticles both in humid and dry conditions. Particles' shapes, sizes, and structures were characterized for these fresh and aged Fe^0-nanoparticles using X-ray diffraction (XRD), X-ray photoelectron spectroscopy, Brunauer−Emmett−Teller surface area and porosity analyzer, transmission electronic microscopy, and energy dispersive X-ray spectroscopy (EDX). Even when aged Fe^0-nanoparticles were exposed to the atmosphere, the Fe^0 content in these aged Fe^0-nanoparticles did not change significantly, which was confirmed by XRD, EDX, and HCl digestion methods. Reactivity of the fresh Fe^0-nanoparticles stabilized using inert/pseudoinert gases for bromate reduction was more than 99% in 20 min, much higher than for microsized ZVI. However, for the aged Fe^0-nanoparticles, the reactivity decreased as the aging time increased; the reactivity of Fe^0-nanoparticles stored in humid conditions decreased much more than that of Fe^0-nanoparticles stored in dry conditions. The observed results revealed that recovery and recrystallization occurred in the aged Fe^0-nanoparticles at room temperature instead of the traditional theory that recrystallization and annealing occur at a high temperature; in additional, recovery and recrystallization are the real mechanisms of the loss of reactivity for aged Fe^0-nanoparticles instead of oxidation.

1. Introduction

Fe^0-nanoparticles have been successfully used as materials for removing organic and inorganic pollutants in surface water and groundwater[1−3] for several years. As a strong reductant, Fe^0-nanoparticles can degrade a wide range of pollutants;[4−6] as a catalyst, evidence of potential catalytic pathways has been reported for both micro and nanoscale iron in the reduction of TCE.[5,7,8] The following physical and chemical aspects have greatly contributed to the increasing environmental applications of Fe^0-nanoparticles. Physically, Fe^0-nanoparticle has a substantial smaller particle size and larger surface area compared to microsized Fe^0, which promotes mass transfer to and from its solid surface and increases the adsorption capacity and reactivity for contaminant removal and degradation.[9,10] Chemically, Fe^0-nanoparticle serves as a cost-effective and environmental-benign reductant.[11−13] In actual water treatment and groundwater remediation, this large surface area and small particle size offers the combined advantages of easy mixing and potential reactivity.

Generally, Fe^0-nanoparticles have been generated in two ways. (1) Reduction of iron oxide using hydrogen gas at temperature around 200−600 °C, and the synthesized Fe^0-nanoparticles are then stabilized and cooled to room temperature using nitrogen gas;[14] and (2) reduction of ferric or ferrous ions using sodium borohydride in liquid phase. The obtained black slurry is dried in several ways. As examples, Glavee heated the slurry under a vacuum at 450 °C,[15] Ponder dried a slurry in a vacuum condition and slowly reintroduced atmosphere to the vacuum to allow the heat generated by the reaction to dissipate,[16] and Liu dried Fe^0-nanoparticles under a vacuum in a glovebox air block or in an oven at 105 °C in nitrogen at 1 atm, and air was then allowed to bleed into the oven slowly overnight.[8] In addition, Hoch reported that his slurry products were heated to 800 °C and held at that temperature for 3 h before being allowed to cool using argon gas.[17]

However, one problem with the above methods is that high temperature will crystallize the structure of Fe^0-nanoparticles, which then decreases the reactivity of these particles for pollutant removal.[5] Moreover, though vacuum drying at room temperature can maintain amorphous structure of Fe^0-nanoparticles, it can cause the sample to rapidly ignite or become oxide once exposed to atmospheric oxygen.[18,19] As such, to overcome this problem, we need to find a convenient and effective method to reduce the crystallization and oxidation of Fe^0-nanoparticles after drying.

Aging effect was recently tested for Fe^0, iron oxide, and Fe/Pd bimetallic nanoparticles to investigate the cause of loss of particle reactivity. Liu and Sarathy investigated the aging effect on TCE and CCl_4 removal using reactive nanoscale iron particles (RNIP) that were immersed in an aqueous solution at different times.[3,20] Ford tested the aging effect by immersing iron oxide into a water bath at 40−70 °C for 2−6 wk.[21] Zhu aged Fe/Pd bimetallic nanoparticles in water for 24 h and found that their reactivity decreased.[22] On the basis of this bimetallic issue, Zhu discussed the loss of reactivity as being due to Pd dislodgment from the aged Fe/Pd and Pd islets encapsulation during the development of iron oxide film over the aging period. However, the aging effect for Fe^0 or bimetallic nanoparticles exposed to

* To whom correspondence should be addressed. E-mail: hcchoi@gist.ac.kr. Phone: +82-62-970-2441. Fax +82-62-970-2434.
[†] Gwangju Institute of Science and Technology (GIST).
[‡] Korea Institute of Science and Technology.

10.1021/jp909137f
Published on Web 01/15/2010

the atmosphere has not yet been investigated, and the effects of aging on the structure of Fe^0-nanoparticles are not clear either.

As a drinking water contaminant, bromate is commonly associated with ozonation processes during water treatment, where it is formed as a disinfection byproduct (DBP) by the oxidation of naturally occurring bromide.[23] In some areas, the concentration of bromate in drinking water is as high as 127 $\mu g\ L^{-1}$,[24] and the United States Environmental Protection Agency (USEPA) set the current maximum contaminant level (MCL) for bromate at 10 $\mu g\ L^{-1}$.[6] To date, several techniques have been applied in attempts to reduce the levels of bromate in drinking water supplies, including filtration, ultraviolet irradiation, photocatalytic decomposition, arc discharge, coagulation, chemical reduction, biological remediation, membrane bioreactor, and activated carbon adsorption.[23,25−28] To a greater extent, Fe^0-nanoparticles have recently been suggested for effective bromate reduction in drinking water systems; Wang successfully reduced bromate using Fe^0-nanoparticles with a second-order kinetics model.[10]

The objectives of this study are to determine an effective method for reducing oxidation and maintaining the reactivity of Fe^0-nanoparticles after lyophilization once synthesized, and then to investigate the effects of aging on the structure of Fe^0-nanoparticles in terms of their reactivity and possible deactivation for the contaminant removal as well as bromate. Understanding the mechanism of aging effect on the reactivity of Fe^0-nanoparticles might provide a further insight on the catalytic activity of lab-synthesized Fe^0 and bimetallic nanoparticles in environmental applications. Additionally, a detailed structural characterization is essential to understand how the structure of Fe^0-nanoparticles relates to its reactivity. In this study, fresh and aged Fe^0-nanoparticles were synthesized using sodium borohydride reduction method. The particle structure, morphology, and surface area were subsequently characterized using X-ray diffraction (XRD), X-ray photoelectron spectroscopy (XPS), Brunauer−Emmett−Teller (BET) surface area and porosity analyzer, transmission electronic microscopy (TEM) with selected area electron diffraction (SAED), and energy dispersive X-ray spectroscopy (EDX). Finally, the reactivity of fresh and aged Fe^0-nanoparticles was investigated through bromate reduction in water treatment.

2. Experimental Methods

2.1. Materials and Chemicals. The chemical reagents used in this study ($KBrO_3$ (99.8%), and $NaBH_4$ (98%)) were reagent grade obtained from Sigma-Aldrich and were used directly as received without pretreatment unless otherwise specified. Iron(III) chloride ($FeCl_3 \cdot 6H_2O$ (97.0−101.0%)) was supplied from Junsei (Japan), ethanol (99.5%) was purchased from Duksan Chem. (South Korea), and ultrahigh purity compressed inert/pseudoinert gases including Ar, N_2, and CO_2, which were purchased from Shinil Gas products (South Korea). All chemical stock solutions were prepared using doubly deionized water (18 MΩ Milli-Q) and stored at 4 °C.

2.2. Synthesis Procedures. Fe^0-nanoparticles were prepared using a borohydride reduction method.[29,30] Briefly, ferric chloride was dissolved in a 1 L 70% (v/v) aqueous ethanol to prepare Fe^{3+} solution, and the prepared ethanol solution was purged with purified nitrogen gas for 3 h to reduce the concentration of dissolved oxygen from 8.0 to 0.6 mg L^{-1}. Then 0.82 M sodium borohydride solution 80 mL was slowly dropped into the Fe^{3+} solution. In a typical preparation, the Fe^{3+} stock solution was prepared right before use. After synthesis, the Fe^0-nanoparticles slurry was washed 2−3 times using pure ethanol and gathered by centrifuging. After centrifuging, the supernatant was removed and the remaining Fe^0-nanoparticles were dried by lyophilization using freeze-dryer (FD5505, IL Shin Lab Co., Ltd.) for 8 h to evaporate ethanol sufficiently.

2.3. Stabilizing Fe^0-Nanoparticles Using Inert/Pseudoinert Gases and Aging Experiment. After the synthesized Fe^0-nanoparticles were dried, the air valve of freeze-dryer was connected to an inert/pseudoinert gas, such as Ar, N_2, and CO_2, to protect the reactive nanoparticles from self-ignition (Supporting Information Figure S1a); Figure S1b illustrates the process for protecting the Fe^0-nanoparticles using inert/pseudoinert gases. The synthesized Fe^0-nanoparticles were kept in an inert/pseudoinert gas-purged tube, and then the Fe^0-nanoparticles were pulverized for future use. Figure S1c illustrates the morphologies between the Fe^0-nanoparticles stabilized using inert/pseudoinert gases and the Fe^0-nanoparticles directly exposed to the atmosphere after lyophilization, and the burned nanoparticles can be observed obviously. For the aging experiments, the pulverized Fe^0-nanoparticles were further separated into two conditions. In condition A, samples were exposed to the atmosphere (at 85% humidity) to investigate the effect of moisture on the structure of Fe^0-nanoparticles. In condition B, samples were kept in a desiccator to reduce the effects of moisture on the structure and reactivity of Fe^0-nanoparticles.

2.4. Solid-Phase Characterization of Fe^0-Nanoparticles. The fresh and aged Fe^0-nanoparticles were characterized using XRD, XPS, BET surface area analyzer, TEM with SAED, EDX, and HCl digestion methods.

XRD analyses were conducted in an ambient air with Cu Kα using a Rigaku RINT 2000 wide-angle goniometer operated at 40 kV and 40 mA; continuous scans from 5 to 90° 2θ were collected with a step size of 0.01° and a count time of 5 s per step. XPS (Multilab 2000, Thermo Electron Corporation, England) was used for iron nanoparticles analysis to determine the surface composition to a depth of less than 5 nm. BET surface areas were determined from nitrogen physisorption with an ASAP 2020 specific surface area and porosity analyzer (Micromeritics Instrument Corp. U.S.A.), using the BJH (Barrett−Joyner−Halenda) and multipoint BET methods; samples were loaded in an anaerobic container and evacuated at specified temperatures between 353 and 423 K for 6 h before each measurement. High-resolution TEM analyses were performed using a JEOL TEM 2100 FXII with SAED operated at 200 kV, and EDX spectrum of the synthesized Fe^0-nanoparticles was obtained using the same instrument. HCl digestion method was performed by digesting Fe^0-nanoparticles into HCl solution and measuring the generated H_2 (g).[3,8]

2.5. Aging Effect on the Reactivity of Fe^0-Nanoparticles. Experiments evaluating the aging effect on the reactivity of fresh and aged Fe^0-nanoparticles on bromate reduction were conducted in a batch system. For bromate reduction, each Teflon-capped 43 mL glass vial containing 4.3 mg fresh or aged Fe^0-nanoparticles was added with prepared bromate stock solution, leaving no head space and resulting in an initial bromate concentration of 1 mg L^{-1}; the Fe^0-nanoparticles dosage of about 0.1 g L^{-1} was much lower than the microsized zero-valent iron (ZVI) dosage of between 25 and 100 g L^{-1} that were used for bromate reduction.[6] The tests were initiated using an end-over-end rotator (at 45 rpm) immediately after the addition of reactants into the vials. Samples were collected after 20 min reaction and subjected to measurements to determine bromate levels after filtration. After a series of reaction time the supernatant solution was analyzed using the same method with the previous report.[10]

TABLE 1: Summary of Physicochemical Properties of Fresh and Aged Fe^0-Nanoparticles

sample name/sampling process		particle size from TEM (nm)	shell thickness (nm)	TEM structure	BET surface area ($m^2\ g^{-1}$)	total Fe content (wt %)	Fe^0 content (wt %)	B content (wt %)
Fe^{Ar}/as received, stabilized using Ar		3−30	3.5−6	irregular Fe^0 core + oxide shell	40.83 ± 0.23	95.1	92.8	4.32
$Fe^{Ar,a}$	humid	6−45	9−13.5	irregular Fe^0 core + thicker oxide shell with clear spots and sharp rings	none measured	92.3/94.0[b]	89.6/90.3[b]	4.95/4.63[b]
	dry	7−45	5−10	irregular Fe^0 core + a little thicker oxide shell with subtle spots and dull rings	none measured	92.5/93.3[b]	90.1/91.0[b]	4.81/4.71[b]
Fe^{N_2}/as received, stabilized using N_2		6−25	2.5−4	irregular Fe^0 core + oxide shell	47.49 ± 0.33	91.5	89.4	4.16
$Fe^{N_2,a}$	humid	8−40	6−13	irregular Fe^0 core + thicker oxide shell with clear spots and sharp rings	none measured	90.8/90.8[b]	87.8/88.0[b]	4.57/4.31[b]
	dry	5−40	5−10	irregular Fe^0 core + a little thicker oxide shell with subtle spots and dull rings	none measured	91.1/91.3[b]	88.4/88.7[b]	4.73/4.50[b]
Fe^{CO_2}/as received, stabilized using CO_2		8−35	3−6	irregular Fe^0 core + oxide shell	45.23 ± 0.25	88.7	84.6	4.09
$Fe^{CO_2,a}$	humid	12−50	8−18	irregular Fe^0 core + thicker oxide shell with clear spots and sharp rings	none measured	78.6/82.8[b]	70.7/72.1[b]	4.78/4.41[b]
	dry	10−40	5−13	irregular Fe^0 core + a little thicker oxide shell with subtle spots and dull rings	none measured	79.1/84.1[b]	71.1/74.6[b]	4.72/4.42[b]

[a] Aging time is 1 month. [b] Aging time is 10 days; humid, aged in a humid condition with a humidity of 85%; dry, aged in a dry condition with a humidity of 15%.

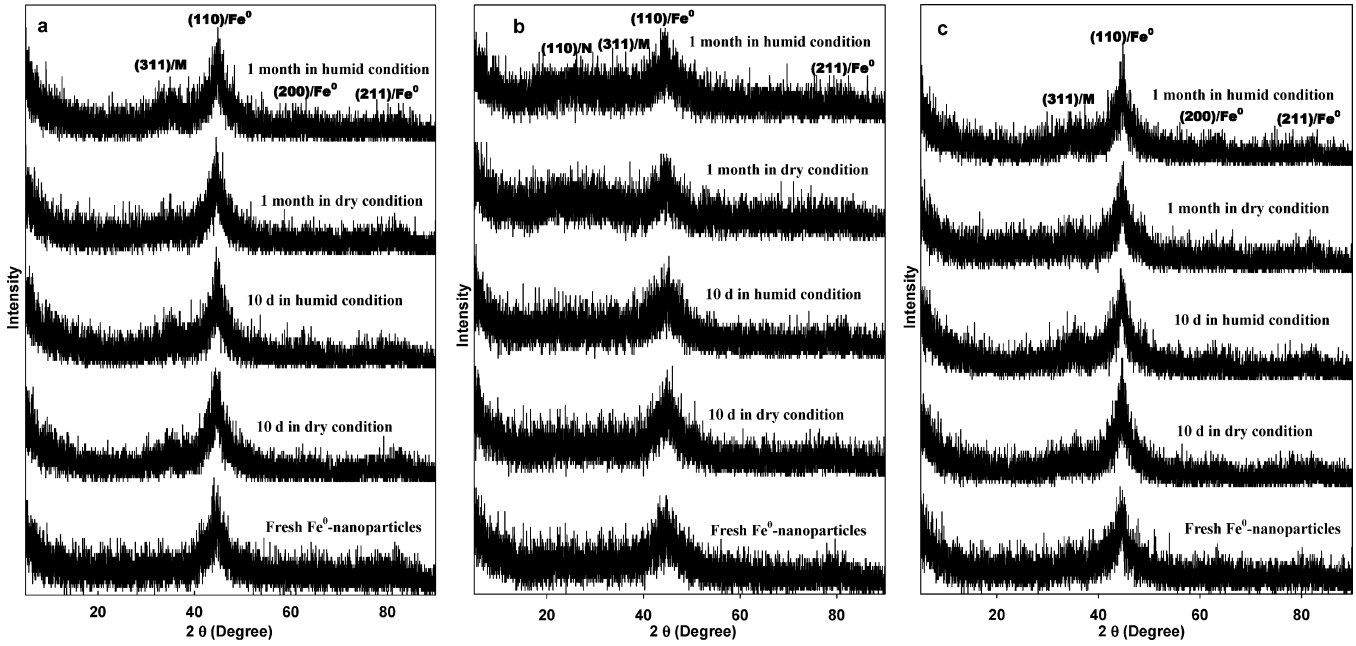

Figure 1. XRD analysis of stabilized fresh and aged Fe^0-nanoparticles. (a) Fe^0-nanoparticles stabilized using Ar, (b) Fe^0-nanoparticles stabilized using N_2, and (c) Fe^0-nanoparticles stabilized using CO_2. Peaks are due to magnetite/maghemite (M), iron oxide hydroxide (N), and Fe^0, respectively.

3. Results and Discussion

3.1. Structure and Composition. Particle's shape, size, composition, and structure are important properties that affect the chemical and physical properties of nanoparticles. To provide primary characterization of these properties, XRD, XPS, and TEM measurements were performed on specimens of fresh and aged Fe^0-nanoparticles as received; BET and EDX measurements were performed on selected samples. The results of these analyses are summarized in Table 1.

XRD analysis of the fresh Fe^0-nanoparticles stabilized using Ar, N_2, and CO_2 showed broad peaks for α-Fe^0 and iron oxide/hydroxide (Figure 1). For Fe^0-nanoparticles stabilized using Ar (Figure 1a), the broad peaks at the 2θ of 44.6, 65, and 82.3° revealed the small particles size and size distributions of α-Fe^0 with indexes of (110), (200), and (211) (JCPDS No. 06-0696). In addition, for fresh Fe^0-nanoparticles stabilized using N_2 and CO_2, XRD analysis revealed similar results as Fe^0-nanoparticles stabilized using Ar (Figure 1b,c). For Fe^0-nanoparticles aged for 10 d and 1 month in a desiccator/dry condition, XRD analysis revealed the broad iron oxide peaks at 26 to 28° and 32 to 36° 2θ with low intensities and strong Fe^0 peak still existing at 44.6° 2θ. The oxidation of Fe^0 by the atmospheric O_2 led to the formation of iron oxide on the surface of the aged Fe^0-nanoparticles; however, this reaction did not significantly change the intensity of Fe^0 in the aged Fe^0-nanoparticles.

For the Fe^0-nanoparticles aged for 10 d and 1 month in the atmosphere/humid condition, XRD analysis revealed more iron oxides peaks with higher intensities with index of (311) (JCPDS

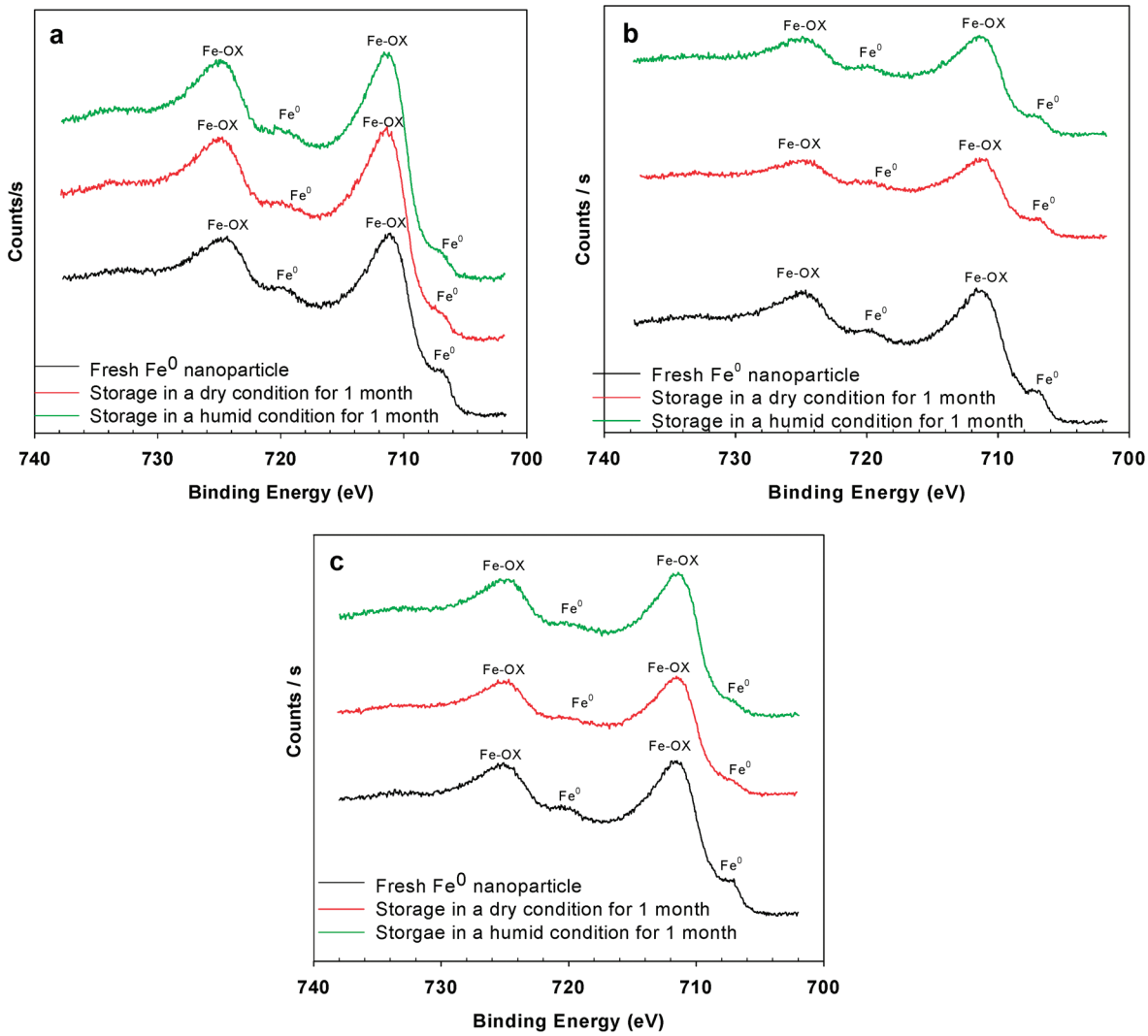

Figure 2. XPS analysis of stabilized fresh and aged Fe^0-nanoparticles. (a) Fe^0-nanoparticles stabilized using Ar, (b) Fe^0-nanoparticles stabilized using N_2, and (c) Fe^0-nanoparticles stabilized using CO_2.

No. 19-0629) than that in the dry condition, thus implying that the aged Fe^0-nanoparticles in humid conditions might be more oxidized than in dry conditions. This phenomenon indicates that the water content in the atmosphere may enhance the oxidation of Fe^0; however, this enhancement did not significantly change the intensity of α-Fe^0 in the Fe^0-nanoparticles.

The Fe_{2p} XPS data were used to determine the Fe^0 and iron oxide content on the surface of fresh Fe^0-nanoparticles stabilized using Ar, N_2, and CO_2 and one month-aged Fe^0-nanoparticles (Figure 2). It showed that the strength of the Fe^0 peak varies with the aging time. For the fresh Fe^0-nanoparticles, a clear peak at around 706.6 eV implies the presence of Fe^0 on the surface; however, for aged Fe^0-nanoparticles, the $2p_{3/2}$ peak of Fe^0 decreased, for the aged Fe^0-nanoparticles stabilized using CO_2, the Fe^0 peaks almost disappeared. Because XPS is sensitive to the outer 3−5 nm of the particles,[31] the presence of a Fe^0 peak confirms that the shell is less than a few nanometers thick. However, exposure of the nanoparticles to the atmosphere caused oxidation at the Fe^0-nanoparticle surface, inducing the Fe^0 peak in the XPS spectra to decrease or disappear. In addition, CO_2 easily reacts with atmospheric water to generate carbonic acid, potentially enhancing the oxidation of Fe^0-nanoparticles on the surface compared to the atmospheric oxygen or water only; therefore, the Fe^0 content at the surface of Fe^0-nanoparticles stabilized using CO_2 is less than that of the Fe^0-nanoparticles stabilized using Ar and N_2.

Specific surface areas of nanoparticles were determined based on the classic BET method using the N_2 adsorption−desorption isotherm of fresh Fe^0-nanoparticles stabilized using Ar, N_2, and CO_2; the measured BET surface areas are shown in Table 1.

Figure S2 (Supporting Information) presents high-resolution TEM images that illustrate the particle size and morphology of the fresh Fe^0-nanoparticles and one month-aged Fe^0-nanoparticles. The TEM images of the three fresh Fe^0-nanoparticles appear similar to one another; the particles appear to have an irregular shape of Fe^0-nanoparticles, a core−shell structure, and a clear contrast between core and shell is evident. There is a notable absence of a lattice fringe and diffuse rings in SAED pattern, indicating that the particles are poorly ordered and amorphous; similar results were further confirmed by the broad peaks in XRD analysis. However, for the aged Fe^0-nanoparticles, the core−shell structure became blurry and the shell thickness increased compared to the fresh Fe^0-nanoparticles. Additionally, we found that the shell of aged Fe^0-nanoparticles stored in humid conditions was significantly thicker than the aged Fe^0-nanoparticles stored in dry conditions (Table 1), due to the increased oxidation of Fe^0-nanoparticles at surface by the atmospheric water.

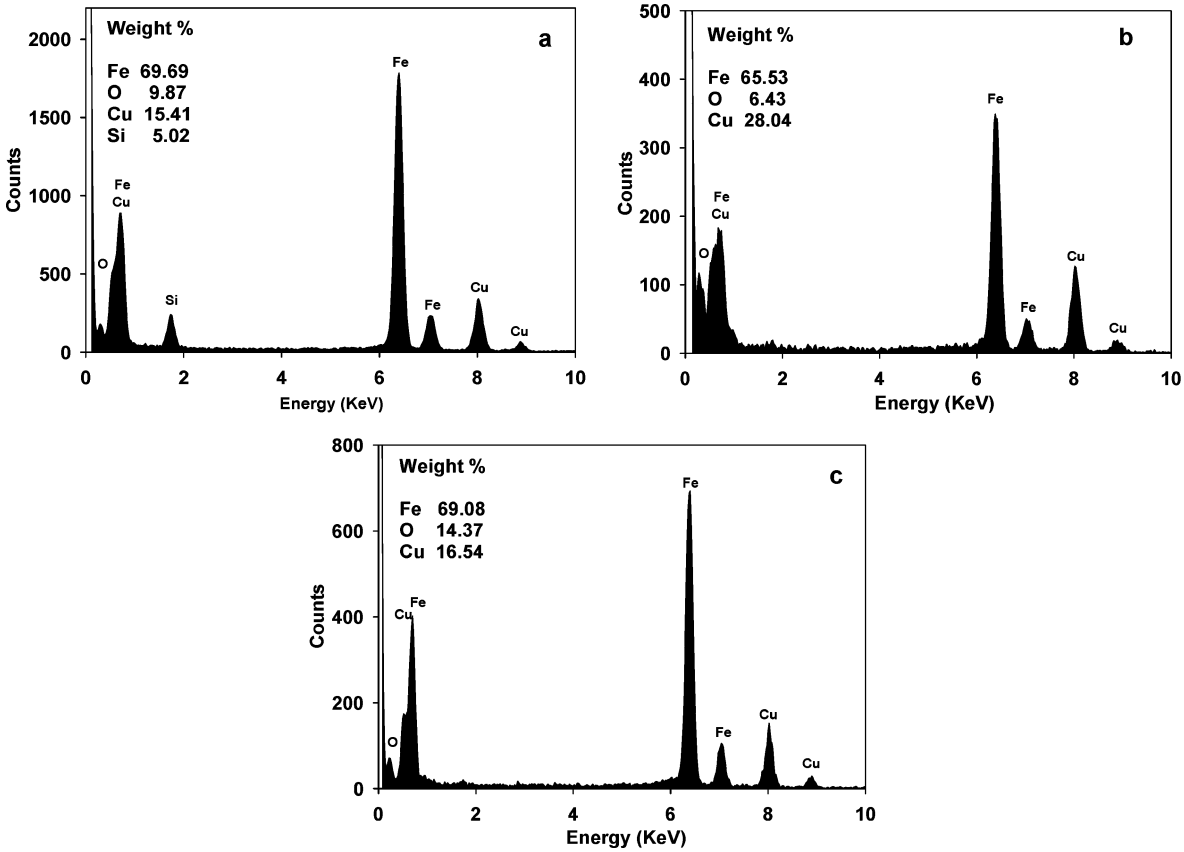

Figure 3. TEM-EDX patterns of stabilized fresh and aged Fe^0-nanoparticles. (a) Fresh Fe^0-nanoparticles stabilized using Ar, (b) 1 month aged Fe^0-nanoparticles of (a) in a dry condition, and (c) 1 month aged Fe^0-nanoparticles of (a) in a humid condition.

The presence of small metal crystallites and nearly crystal structures were observed in the aged Fe^0-nanoparticles stored in humid conditions. In addition, clear spots and sharp rings on the SAED patterns further confirmed the presence of ordered and crystalline structures generated from the aged Fe^0-nanoparticles; the irregular spacing and structural dislocation of the observed lattice planes indicate that the aged Fe^0-nanoparticles are polycrystalline. The corresponding SAED patterns (inset in Supporting Information Figure S2a2,a3,b2,b3,c2,c3) show the presence of (311), (110), (200), and (211) planes of the aged Fe^0-nanoparticles. Moreover, the intensity of clear spots and sharp rings of Fe^0-nanoparticles in humid conditions is much higher than that of Fe^0-nanoparticles stored in dry conditions, thus verifying that the degree of crystallization in Fe^0-nanoparticles stored in humid conditions is higher than the Fe^0-nanoparticles stored in dry conditions. Compared to the SAED of fresh Fe^0-nanoparticles, the intensities of (110), (200), and (211) planes for Fe^0 became higher and the plane of (311) for iron oxide generated in aged Fe^0-nanoparticles, indicating occurrences of recrystallization in aged Fe^0-nanoparticles; additionally, the generated iron oxides were also recrystallized in aged Fe^0-nanoparticles.

The chemical compositions of the fresh and 1 month-aged Fe^0-nanoparticles stabilized using Ar were determined using EDX spectra analysis (Figure 3). In the EDX spectra, except for the copper and silicon signals from the TEM grid, peaks for Fe and O are observed; however, it could be noted that the composition of elements between fresh and aged Fe^0-nanoparticles were not significantly different, indicating that the iron oxide content in aged Fe^0-nanoparticles did not increase significantly comparing to fresh Fe^0-nanoparticles, which is consistent with the XRD results.

The Fe^0 contents of fresh and aged Fe^0-nanoparticles were determined using HCl digestion method and shown in Table 1. Similar results with XRD for Fe^0 content were obtained in Fe^0-nanoparticles stabilized using Ar, N_2, and CO_2. The less Fe^0 content in Fe^0-nanoparticles stabilized using CO_2 was due to the surface oxidation by carbonic acid.

Thus, the observed EDX, XRD, XPS, and HCl digestion results indicate that the oxidation of Fe^0 only occurred at the surface of aged Fe^0-nanoparticles, the core of aged Fe^0-nanoparticles still maintains Fe^0.

3.2. Aging Effect on the Structure of Fe^0-Nanoparticles. From the SAED pattern we found that the degree of poorly order in aged Fe^0-nanoparticles decreased compared to the fresh Fe^0-nanoparticles. In particular, the presence of metal crystallites, clear spots, and sharp rings were notably observed in the Fe^0-nanoparticles stored in humid conditions at room temperature, significantly different from the traditional theory that high temperature is one of the major conditions for increasing the crystallinity for poorly ordered materials as well as Fe^0.[5,32,33] The observed phenomenon indicates that recovery, a process by which deformed grains can reduce their stored energy through the removal or rearrangement of defects in their crystal structure, and recrystallization happen in the aged Fe^0-nanoparticles that initially have amorphous structure once synthesized.[34−36] This change of structure, including recovery and recrystallization, can be described into three steps.[37] First, the amorphous Fe^0-nanoparticles contain numerous dislocations that are mainly captured in "tangles" (Figure 4a). Amorphous Fe^0-nanoparticles with high stacking fault energy tend to form a cellular structure in which the rough tangles of dislocation are contained on the cell walls. Related reduced dislocation density is obtained in the cells. Note that dislocations are related to specific strain

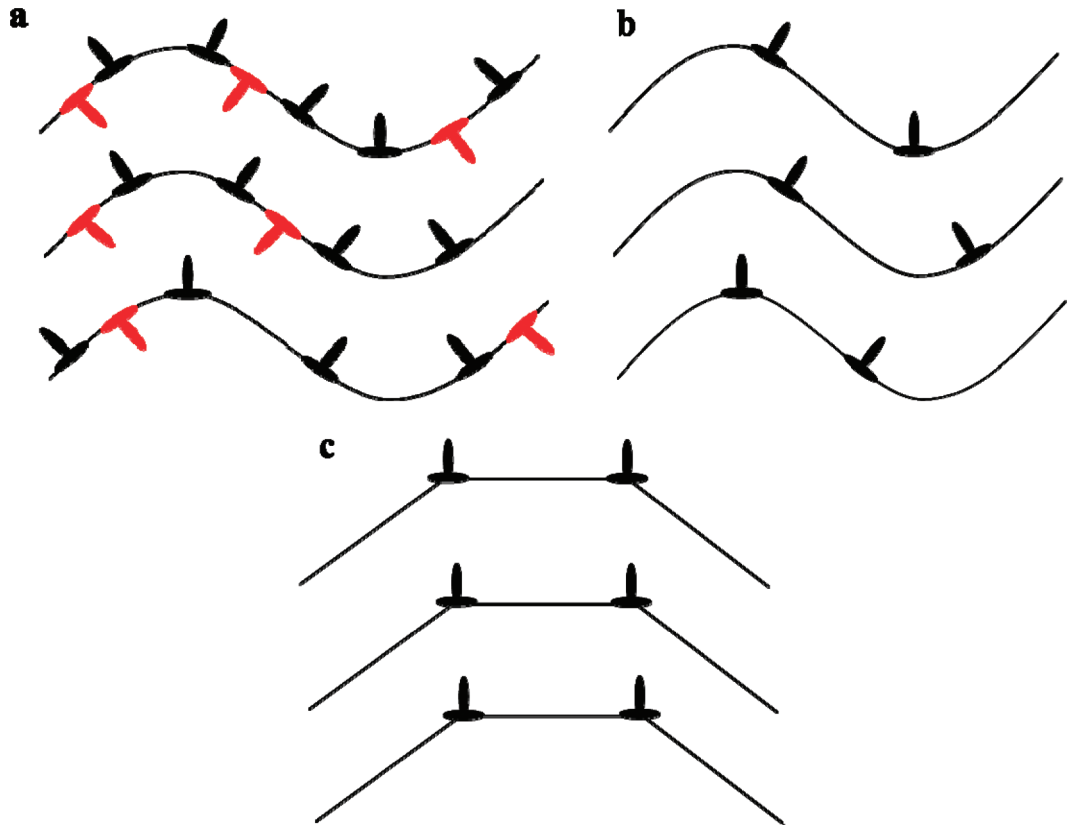

Figure 4. The annihilation and reorganization of an array of edge dislocations in a crystal lattice (a) Bent lattice with dislocations of both sign, (b) annihilation of dislocations with opposite sign, and (c) polygonization of the lattice.

fields that supply finite amount stored energy to the material. In addition, these dislocations tend to become more movable as increasing the temperature, thereby enabling them to slide and ascend. However, in the case that dislocations of opposite signs congregate, they effectively counteract each other and their contribution to the stored energy is eliminated; when this process is complete, the extra dislocations of one type will remain (Figure 4b). Finally, any excess dislocations will arrange themselves into ordered arrays in which their participations to the stored energy are lessened through the overlapping of their strain fields (Figure 4c). Thermodynamically, the energy stored in the amorphous structure of Fe^0-nanoparticles is much higher than that in the crystalline structure due to the small particle size; the stored surface energy is also higher than bulk-sized ZVI. In addition, the oxidation of Fe^0-nanoparticles is an exothermic reaction. Therefore, when Fe^0-nanoparticles are oxidized by atmospheric O_2 or water at room temperature, the local oxidized Fe^0-nanoparticles emit heat, and simultaneously lose their stored energy. This thermodynamical process enhances the recovery and recrystallization of the Fe^0-nanoparticles; the energetically unstable amorphous structure is ultimately replaced by a stable crystalline phase.

3.3. Aging Effect on the Reactivity of Fe^0-Nanoparticles. Reactivity of fresh and aged Fe^0-nanoparticles was investigated through bromate reduction. Figure 5 shows the bromate reduction efficiency of fresh, aged, and fresh Fe^0-nanoparticles without inert/pseudoinert gases stabilization. It was found that bromate could be effectively reduced more than 99% in 20 min using fresh Fe^0-nanoparticles stabilized using argon, nitrogen, and carbon dioxide, much higher than the 58% bromate reduction efficiency of fresh Fe^0-nanoparticles directly exposed to the atmosphere (Figure 5a) and microsized ZVI.[6] This higher reactivity is due to the higher surface area and amorphous structure compared to microsized ZVI with a lower surface area and a crystalline structure;[6,31] similar results were reported for TCE removal.[5] However, for bromate reduction using aged Fe^0-nanoparticles, the bromate reduction efficiency decreased as aging time increased (Figure 5a−c). In addition, the bromate reduction efficiency using aged Fe^0-nanoparticles stored in humid conditions was significantly lower than that of Fe^0-nanoparticles; moreover, the bromate reduction efficiency is still maintained at more than 50% using Fe^0-nanoparticles stored in dry conditions. This result was partially due to the oxidation on the surface of the Fe^0-nanoparticles, which was confirmed by XPS results (Figure 2); additionally, recovery and recrystallization of aged Fe^0-nanoparticles stored in humid conditions was higher than that of aged Fe^0-nanoparticles stored in dry conditions, which significantly decreased particles' reactivity compared to amorphous Fe^0.[5] Finally, it was determined that the bromate reduction efficiency of aged Fe^0-nanoparticles that was initially stabilized using CO_2 decreased more than that of other aged Fe^0-nanoparticles (Figure 5c), which is due to the formation of carbonic acid that results in higher levels of oxidation at surface and more recovery and recrystallization than other Fe^0-nanoparticles, as revealed by the XPS results and SAED patterns.

4. Conclusions

Lab synthesized Fe^0-nanoparticles were stabilized to prevent from self-ignition after lyophilization using inert/pseudoinert gases. For aged Fe^0-nanoparticles, it was subsequently found that the Fe^0 content was not influenced significantly compared to the fresh synthesized Fe^0-nanoparticles, and the recovery and recrystallization occurred in the Fe^0-nanoparticles structure at room temperature. The reactivity of synthesized Fe^0-nanopar-

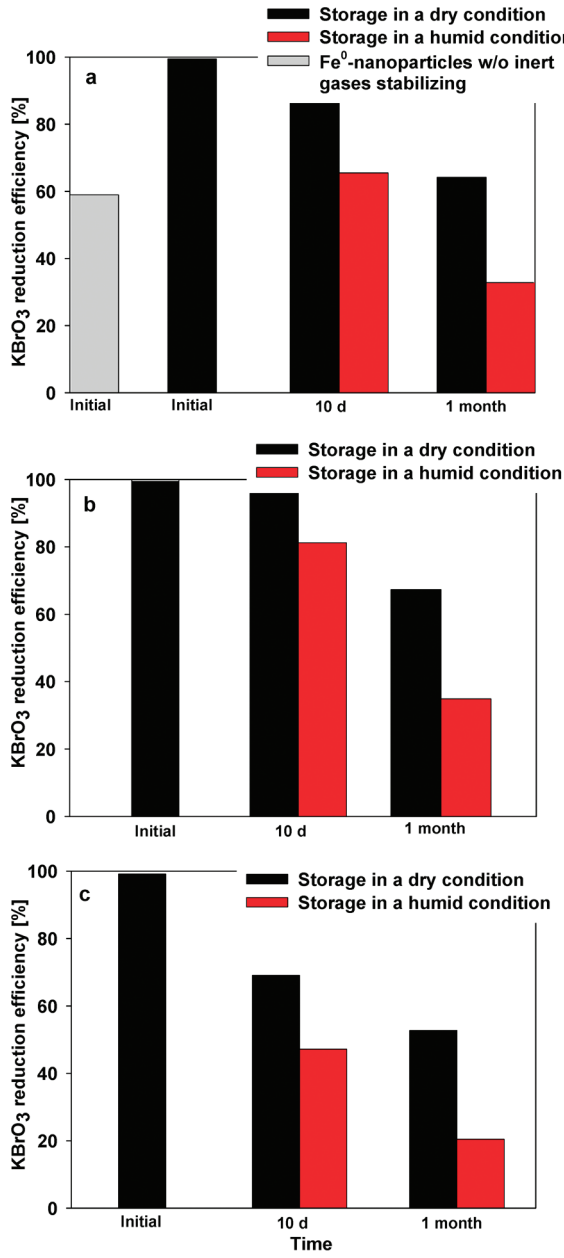

Figure 5. Bromate reduction using stabilized fresh and aged Fe^0-nanoparticles. (a) Fe^0-nanoparticles stabilized using Ar, (b) Fe^0-nanoparticles stabilized using N_2, and (c) Fe^0-nanoparticles stabilized using CO_2.

ticles stabilized using inert/pseudoinert gases was found to be higher than that of Fe^0-nanoparticles directly exposed to the atmosphere and microsized ZVI for bromate reduction. In addition, as aging time increased, the reactivity of Fe^0-nanoparticles stored in humid conditions decreased much more than that of Fe^0-nanoparticles stored in dry conditions, as the intensity of recovery and recrystallization in humid conditions is higher than that in dry conditions.

Acknowledgment. This work was supported by the Korea Ministry of Education, Science, and Technology, through the National Research Laboratory Program and partially supported by the Korea Science and Engineering Foundation (KOSEF). We greatly appreciate Professor Zhonglin Wang (Georgia Tech) and Professor Qing Yang (USTC) for their constructive suggestions in nanoparticles characterization.

Supporting Information Available: Two figures show additional details of our analysis. This material is available free of charge via the Internet at http://pubs.acs.org.

References and Notes

(1) Giasuddin, A. B. M.; Kanel, S. R.; Choi, H. *Environ. Sci. Technol.* **2007**, *41*, 2022.
(2) Kanel, S. R.; Manning, B.; Charlet, L.; Choi, H. *Environ. Sci. Technol.* **2005**, *39*, 1291.
(3) Liu, Y. Q.; Lowry, G. V. *Environ. Sci. Technol.* **2006**, *40*, 6085.
(4) Choe, S.; Chang, Y. Y.; Hwang, K. Y.; Khim, J. *Chemosphere* **2000**, *41*, 1307.
(5) Liu, Y.; Choi, H.; Dionysiou, D.; Lowry, G. V. *Chem. Mater.* **2005**, *17*, 5315.
(6) Xie, L.; Shang, C. *Chemosphere* **2007**, *66*, 1652.
(7) Farrell, J.; Melitas, N.; Kason, M.; Li, T. *Environ. Sci. Technol.* **2000**, *34*, 2549.
(8) Liu, Y.; Majetich, S. A.; Tilton, R. D.; Sholl, D. S.; Lowry, G. V. *Environ. Sci. Technol.* **2005**, *39*, 1338.
(9) Campbell, C. T.; Parker, S. C.; Starr, D. E. *Science* **2002**, *298*, 811.
(10) Wang, Q.; Snyder, S.; Kim, J.; Choi, H. *Environ. Sci. Technol.* **2009**, *43*, 3292.
(11) Masciangioli, T.; Zhang, W. X. *Environ. Sci. Technol.* **2003**, *37*, 102A.
(12) Zhang, W -x. *J. Nanopart. Res.* **2003**, *5*, 323.
(13) Phenrat, T.; Saleh, N.; Sirk, K.; Kim, H. J.; Tilton, R. D.; Lowry, G. V. *J. Nanopart. Res.* **2008**, *10*, 795.
(14) Uegami, M.; Kawano, J.; Okita, T.; Fujiii, Y.; Okinaka, K.; Kakuya, K.; Yatagai, S. *U.S. Patent Application 20030217974A1*, 2003.
(15) Glavee, G. N.; Klabunde, K. J.; Sorensen, C. M.; Hadjipanayis, G. C. *Inorg. Chem.* **1995**, *34*, 28.
(16) Ponder, S. M.; Darab, J. G.; Mallouk, T. E. *Environ. Sci. Technol.* **2000**, *34*, 2564.
(17) Hoch, L. B.; Mack, E. J.; Hydutsky, B. W.; Hershman, J. M.; Skluzacek, J. M.; Mallouk, T. E. *Environ. Sci. Technol.* **2008**, *42*, 2600.
(18) Celebi, O.; Uzum, C.; Shahwan, T.; Erten, H. N. *J. Hazard. Mater.* **2007**, *148*, 761.
(19) Sohn, K.; Kang, S. W.; Ahn, S.; Woo, M.; Yang, S.-K. *Environ. Sci. Technol.* **2006**, *40*, 5514.
(20) Sarathy, V.; Tratnyek, P. G.; Nurmi, J. T.; Baer, D. R.; Amonette, J. E.; Chun, C. L.; Penn, R. L.; Reardon, E. J. *J. Phys. Chem. C.* **2008**, *112*, 2286.
(21) Ford, R. G.; Bertsch, P. M.; Farley, K. J. *Environ. Sci. Technol.* **1997**, *31*, 2028.
(22) Zhu, B.-W.; Lim, T.-T. *Environ. Sci. Technol.* **2007**, *41*, 7523.
(23) Butler, R.; Ehrenberg, S.; Godley, A. R.; Lake, R.; Lytton, L.; Cartmell, E. *Sci. Total Environ.* **2006**, *366*, 12.
(24) Mari, A.; Takako, A. *J. Health Sci.* **1999**, *45*, 344.
(25) Asami, M.; Aizawa, T.; Morioka, T.; Nishijima, W.; Tabata, A.; Magara, Y. *Water Res.* **1999**, *33*, 2797.
(26) Hijnen, W. A. M.; Jong, R.; Van der Kooij, D. *Water Res.* **1999**, *33*, 1049.
(27) Mills, A.; Belghazi, A.; Rodman, D. *Water Res.* **1996**, *30*, 1973.
(28) Noguchi, H.; Nakajima, A.; Watanabe, T.; Hashimoto, K. *Water Sci. Technol.* **2002**, *46*, 27.
(29) Wang, Q.; Choi, H. *Environ. Sci. Technol.* **2008**, *42*, 3479.
(30) Wang, Q.; Kanel, S. R.; Park, H.; Ryu, A.; Choi, H. *J. Nanopart. Res.* **2009**, *11*, 749.
(31) Nurmi, J. T.; Tratnyek, P. G.; Sarathy, V.; Baer, D. R.; Amonette, J. E.; Pecher, K.; Wang, C.; Linehan, J. C.; Matson, D. W.; Penn, R. L.; Driessen, M. D. *Environ. Sci. Technol.* **2005**, *39*, 1221.
(32) Van Wonterghem, J.; Morup, S.; Koch, C. J. W.; Charles, S. W.; Wells, S. *Nature* **1986**, *322*, 622.
(33) Hu, Z.; Fan, Y.; Wu, Y.; Yan, Q.; Chen, Y. *J. Mater. Sci.* **1996**, *31*, 611.
(34) Doherty, R. D. *Encyclpedia of Materials: Science and Technology*; Elsevier: New York, 2005; p 7847.
(35) Doherty, R. D.; Hughes, D. A.; Humphreys, F. J.; Jonas, J. J.; Jenson, D. J.; Kassner, M. E.; King, W. E.; McNelley, T. R.; McQueen, H. J.; Rollett, A. D. *Mater. Sci. Eng. A-Struct. Mater. Prop. Microstruct. Process.* **1997**, *238*, 219.
(36) Kappes, B. B.; Meacham, B. E.; Tang, Y. L.; Branagan, D. J. *Nanotechnology* **2003**, *14*, 1228.
(37) http://en.wikipedia.org/wiki/Recovery_(metallurgy).

JP909137F